Editors' Suggestion

Dirac Spin Liquid on the Spin-1/2 Triangular Heisenberg Antiferromagnet

Shijie Hu,[1,*] W. Zhu,[2,†] Sebastian Eggert,[1] and Yin-Chen He[3,‡]

[1]*Department of Physics and Research Center Optimas, Technische Universitat Kaiserslautern, 67663 Kaiserslautern, Germany*

[2]*Institute of Natural Sciences, Westlake Institute of Advanced Study, School of Science, Westlake University, Hangzhou, 030024, People's Republic of China*

[3]*Perimeter Institute for Theoretical Physics, Waterloo, Ontario N2L 2Y5, Canada*

(Received 12 June 2019; revised manuscript received 27 September 2019; published 15 November 2019)

We study the spin liquid candidate of the spin-1/2 J_1-J_2 Heisenberg antiferromagnet on the triangular lattice by means of density matrix renormalization group (DMRG) simulations. By applying an external Aharonov-Bohm flux insertion in an infinitely long cylinder, we find unambiguous evidence for gapless $U(1)$ Dirac spin liquid behavior. The flux insertion overcomes the finite size restriction for energy gaps and clearly shows gapless behavior at the expected wave vectors. Using the DMRG transfer matrix, the low-lying excitation spectrum can be extracted, which shows characteristic Dirac cone structures of both spinon-bilinear and monopole excitations. Finally, we confirm that the entanglement entropy follows the predicted universal response under the flux insertion.

DOI: 10.1103/PhysRevLett.123.207203

Introduction.—Quantum spin liquids (QSLs) are exotic phases of matter which remain disordered due to quantum fluctuations which, in turn, give rise to remarkable properties of fundamental importance, such as fractionalizations, gauge fluctuations, topology, and unconventional superconductivity [1–4]. However, despite of a long-running quest, theoretical and experimentally relevant models for enigmatic QSLs are still limited and rare.

Historically, it has been proposed that geometric frustrations on the spin-1/2 triangular antiferromagnetic Heisenberg model (TAFM) could lead to a spin disordered ground state [5]. Although the nearest neighbor TAFM turns out to exhibit a 120° magnetic order [6–10], the possibility of increasing the frustration by adding next-nearest-neighbor (NNN) interactions has captured much interest in the literature [11–26] for the J_1-J_2 TAFM

$$H = J_1 \sum_{\langle i,j \rangle} \mathbf{S}_i \cdot \mathbf{S}_j + J_2 \sum_{\langle\langle i,j \rangle\rangle} \mathbf{S}_i \cdot \mathbf{S}_j, \qquad (1)$$

where $\langle i,j \rangle$ and $\langle\langle i,j \rangle\rangle$, respectively, denote NN and NNN bonds. So far, the general consensus is that an intermediate region ($0.07 \lesssim J_2/J_1 \lesssim 0.15$) without magnetic ordering [11–24] is sandwiched between a stripe ordered phase ($J_2/J_1 \gtrsim 0.15$) [25,26] and a 120° magnetically ordered phase ($0.0 \leq J_2/J_1 \lesssim 0.07$) [6–10]. However, the underlying physics and precise nature of this intermediate phase is under an intense debate. For instance, variational Monte Carlo simulations suggest a gapless $U(1)$ Dirac QSL [14] as candidates for this intermediate phase. Density-matrix renormalization group (DMRG) calculations [16–19] found an indication of a gapped QSL as the nonmagnetic phase, while its internal structure (e.g., Z_2, chiral) has yet to be determined. In addition, extensive exact diagonalization calculations fail to find evidence in support of either theory in the accessible system sizes [20]. Taken as a whole, although a possible QSL phase has been identified on TAFM, the exact nature of this intermediate phase remains elusive.

It was shown that other experimental-relevant spin models on the triangular lattice also show spin liquid behavior which is continuously connected to the spin-liquid phase of the J_1-J_2 TAFM model [27,28]. Thus, understanding the underlying physics in the J_1-J_2 TAFM, will give deep insight into a whole class of new triangular materials, for example, the recent synthesized Na-based chalcogenides [29–33]. In particular, the spin dynamics of $NaYbO_2$ shows low-energy spectral weight accumulating at the K point of the Brillouin zone [31]. So far, it is unclear if these findings can be interpreted within the spin liquid picture [34,35], which demonstrates the need for detailed theoretical predictions.

In this Letter, we unveil the QSL nature of the triangular J_1-J_2 model by using large-scale DMRG simulations armed with recently developed state-of-the-art transfer matrix analysis [36,37]. We find smoking-gun signatures of the $U(1)$ Dirac QSL (DSL), which consistently appear in 16 different geometries and/or system sizes [see Fig. 1(a) for details]. These signatures include (1) momentum-dependent "excitation spectra," extracted from the DMRG transfer matrix [36,37], which reveals gapless modes of the Dirac spin liquid showing recently predicted behavior of both fermion bilinear excitations as well as intricate monopoles [34,35], (2) strong dependence of the energy

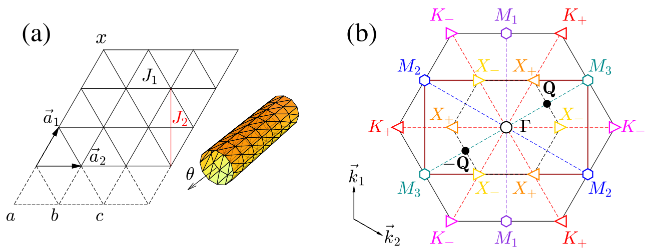

FIG. 1. Geometry of cylinders in real space and momentum points in the first Brillouin zone. (a) Three different cylindrical geometries, YC4-0, YC4-1, or YC4-2 [39], which correspond to identifying site x with site a, b, or c, respectively. We also insert an Aharonov-Bohm flux in the hole of the cylinder, which modifies the spin exchange terms in Hamiltonian Eq. (1) across the boundary (labeled by dashed lines). (b) The black solid line shows the first Brillouin zone of the triangular lattice while the brown rectangle is the magnetic Brillouin zone due to the π flux in each unit cell seen by spinons. All characteristic points are labeled by (k_1, k_2) modulo 2π. Two Dirac points (black dots) of spinons are located at $\mathbf{Q} = (\pi/2, \pi/2)$ and $-\mathbf{Q}$ (for details see [39]). The gauge invariant excitations, e.g. fermion bilinears and monopoles, are locating at high symmetric points, including $\Gamma = (0, 0)$; $M_1 = (\pm\pi, 0)$ (violet hexagon), $M_2 = (0, \pm\pi)$ (blue hexagon), $M_3 = \pm(\pi, \pi)$ (dark cyan hexagon), $K_+ = (-2\pi/3, 2\pi/3)$ (red left triangle), $K_- = (2\pi/3, -2\pi/3)$ (magenta right triangle); $X_+ = (-\pi/3, \pi/3)$ (orange left triangle), $X_- = (\pi/3, -\pi/3)$ (gold right triangle).

gap on twisted boundary conditions [36], and (3) universal entanglement entropy response under flux insertion [38]. This evidence unambiguously shows that the intermediate phase in TAFM is a gapless $U(1)$ DSL.

Properties of $U(1)$ *DSL.*—Let us begin with a brief review of properties of the $U(1)$ DSL on the triangular lattice [14,34,35,43]. We begin with rewriting the spin operator in terms of fractional fermionic spinons $\boldsymbol{f} = (f_\uparrow, f_\downarrow)^T$, $\boldsymbol{S} = \boldsymbol{f}^\dagger \boldsymbol{\sigma} \boldsymbol{f}$, where the partons $\boldsymbol{f}$ are coupled to a $U(1)$ dynamic gauge field due to the $U(1)$ redundancy. The $U(1)$ DSL can then be realized by putting spinons in a staggered π flux mean-field ansatz, whose band structure will have two Dirac cones located at the $\pm Q$ points [valley, black dots in Fig. 1(b)] of the Brillouin zone [14,39]. The low energy physics of the $U(1)$ DSL is captured by $N_f = 4$ QED_3, namely, there are four Dirac fermions (two from spins $\uparrow/\downarrow$ and two from valleys) coupled to a dynamic $U(1)$ gauge field. This $N_f = 4$ QED_3 theory may flow into a $2+1\mathrm{D}$ conformal field theory (CFT) in the infrared; therefore the $U(1)$ DSL is a critical or conformal phase [44–46], which is a close analog to the familiar spin-1/2 Heisenberg chain in $1+1\mathrm{D}$ [47–49]. One effective way to detect the $U(1)$ DSL is to measure its gapless modes. It has been shown that the $U(1)$ DSL has two types of fundamental gapless modes, namely, fermion (spinon) bilinears and monopoles [of the $U(1)$ gauge field] [34,35,46,50]. The fermion bilinears are "particle-hole" excitations of four Dirac fermions, while monopoles are instantons of the $U(1)$ gauge field. It is worth emphasizing that both fermion bilinears and monopoles are gauge invariant which correspond to local operators such as spin $\boldsymbol{S}$, dimer operators $\boldsymbol{S}_i \cdot \boldsymbol{S}_j$, etc. Moreover, these critical operators have distinct quantum numbers (spins, momentum, angular momentum, etc.), enabling us to detect them directly.

There are, in total, 16 fermion bilinears [45], which can be grouped into $1 \oplus 15$, namely, $SU(4)$ singlet and adjoint. They are distributed at different momenta in the first Brillouin zone (BZ) of the triangular lattice [seen in Fig. 1(b)]. The singlet bilinear is a spin singlet with zero momentum (Γ point, black circle). The 15 adjoint bilinears can be classified into three types [34]: Type (**B1**) three time-reversal-even spin singlets with momenta located at three M points of the BZ: M_1 (violet hexagon), M_2 (blue hexagon), and M_3 (dark-cyan hexagon). Type (**B2**) three time-reversal-even spin triplets with zero momentum located at the Γ points (black circle) of the BZ. Type (**B3**) nine time-reversal-odd spin triplets with momenta located at three M points (hexagon). The quantum numbers of the monopoles in the $U(1)$ DSL remained elusive for decades until recently solved in Refs. [34,35]. There are six monopole operators (which are complex) of two types: Type (**M1**) three time-reversal-odd spin-triplets with momenta located at $K_\pm$ (red left triangle and magenta right triangle). Type (**M2**) three time-reversal-even spin-singlets with momenta located at the $X_\pm$ points (orange left triangle and gold right triangle). Physically, the condensation of spin-triplet monopoles will give the familiar 120° noncollinear magnetic order, while the condensation of spin-singlet monopoles leads to a valence bond solid such as a $\sqrt{12} \times \sqrt{12}$ state [34]. Later, we will show that signatures of both the fermion bilinear and monopole operators have been measured in our DMRG simulations.

Method.—We use infinite-DMRG [51–53] to simulate the J_1-J_2 TAFM wrapped on infinitely long cylinders. The evidence for DSL excitations is based on two major improvements in this Letter. First, we study different types of cylindrical geometries which correspond to different ways of wrapping a cylinder. As shown in Fig. 1(a), we define the $\mathrm{YC}L_y$-n cylinders by identifying the site $\boldsymbol{r}$ with the site $\boldsymbol{r} + L_y \boldsymbol{a}_1 - n \boldsymbol{a}_2$ [39]. For instance, the notation YC8-1 denotes a cylinder (C) with circumference of eight lattice spacing and a shift of one column in the y direction (Y) when connected periodically. Here, $\boldsymbol{a}_{1/2}$ are the triangular Bravais lattice primitive vectors, L_y is the "circumference" of the cylinder, and n amounts to a shift along the cylindrical direction. Simulating different geometries not only proves the observed DSL signatures are robust against finite size effect, but also serves as a nontrivial check as DSLs on different geometries show qualitatively different behaviors (see Supplemental Material [39]). Second, we carry out a numerical Aharonov-Bohm experiment by inserting flux θ in the cylinder, see Fig. 1(a). This is implemented by twisted boundary conditions, which modify interactions crossing the boundary by a phase factor, e.g., $S_i^+ S_j^- e^{i\theta} + S_j^+ S_i^- e^{-i\theta}$ with a flux angle θ [40]. With the flux insertion, we can fully scan the momentum points in the Brillouin zone on a given geometry and, therefore, are not limited by finite-size energy gaps. Furthermore, certain physical quantities in DSLs, such as the entanglement entropy, have a nontrivial response under flux insertion [38].

In the simulation, it is important to keep the ground-state evolving adiabatically under the flux insertion. In most cases, the adiabatic flux insertion can be maintained, except very close to the Dirac cone (large flux θ), where accurate infinite-DMRG simulation becomes very challenging due to the small gap and large entanglement of the state. Once adiabatic flux insertion fails at large θ, the infinite-DMRG simulation may suddenly collapse to a competing state in other superselection sectors of the ground state [39] or a symmetry broken state due to the instability of the gapless state [36]. We will not present the data of flux θ for which adiabatic flux insertion fails, as they do not reveal any direct information of the spin-liquid ground state at zero flux.

Excitation gap.—Previous DMRG studies have found a considerably large spin gap in the J_1-J_2 TAFM [17]. However, this is not sufficient to exclude a DSL since, on a cylinder, the momentum is discrete, so the gapless Dirac point may be missed. The flux insertion, which effectively changes the quantized momentum of spinons, can make spinons hit the Dirac point at specific values of flux θ [36]. By carefully studying the DSL ansatz incorporating the effect of emergent gauge fields [39], we find that DSLs on different cylinder geometries YCL_y-n have distinct θ dependence. If both L_y and n are even, spinons are gapless when $\theta = 2\pi$ (Since spinons are fractional particles, the flux insertion has 4π periodicity). For all of the other three cases, spinons will be gapless at $\theta = \pi$ or 3π.

Figure 2 shows the energy gap as a function of flux θ. Although the gap is large at $\theta = 0$ [54], we find it significantly decreases as θ increases. The sensitivity of the energy gap is an indication of the gapless DSL: (1) for a gapped spin liquid, the spin gap should have a small dependence (exponentially in L_y) on the flux; (2) finite flux drags the momentum lines toward the Dirac points; thus the gap monotonically reduces. Because of the small gap when Dirac points are approached, we are not able to maintain the adiabatic flux insertion when $\theta \sim 1.5\pi$ for the YC2n-2m cylinder, and $\theta \sim \pi$ for all other cylinders. There are also truncation effects from the finite bond dimensions m in infinite-DMRG, which may explain that the YC10-1 gap appears larger than the YC8-1 gap in Fig. 3. We discuss results for different m in the Supplemental Material [39]. We also remark that the gap we measured may come from monopoles (rather than spinons), whose finite size effect is

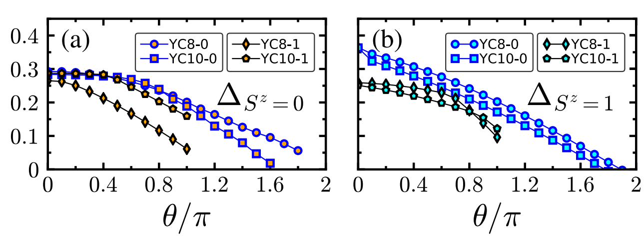

FIG. 2. Spin excitation gap. (a) Energy gap $\Delta_{S^z=0}$ and (b) $\Delta_{S^z=1}$ as a function of the inserted flux θ at $J_2/J_1 = 0.12$ for YC8-0 (blue circles), YC10-0 (blue squares), YC8-1 (black diamonds), and YC10-1 (black pentagon) cylinder geometries. The data are collected using DMRG bond dimension $m = 4096$ for YC8/10-0 and 6144 for YC8/10-1. (For details, please see the Supplemental Material [39]).

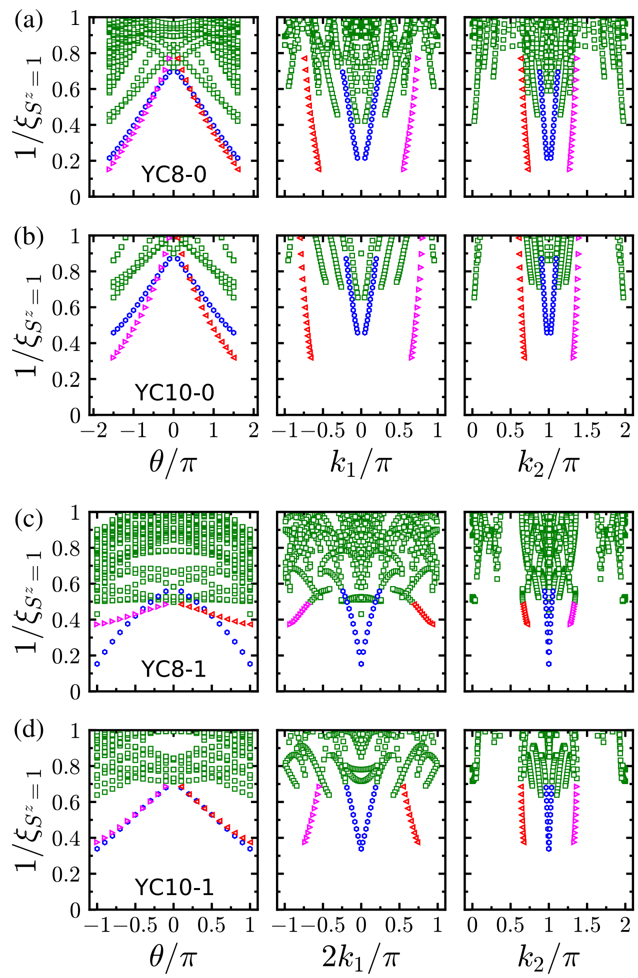

FIG. 3. Correlation length spectrum. Inverse correlation length $1/\xi_{S^z=1}$ as a function of the flux θ (left column), momentum k_1 (middle column), and momentum k_2 (right column) for the cylinder (a) YC8-0, (b) YC10-0, with $m = 6144$ and (c) YC8-1, (d) YC10-1 with $m = 12288$. The lowest-lying excitations contain a spinon pair at M points and monopole excitations at $K_\pm$ points, the former is denoted by the blue hexagon while the latter is denoted by the red left triangle and magenta right triangle. It is an artifact of finite bond dimension that the correlation length is not diverging at the Dirac point, and it becomes more severe for the larger system sizes (see Supplemental Material [39] for more discussion).

more subtle to analyze. The important message to take is, in all cases, the gap systematically decreases as a function of θ, and it is consistent with the theoretical expectation that the finite-size gap of spinons vanishes at (i) $\theta = \pi$ for YC8-1 and YC10-1, (ii) $\theta = 2\pi$ for YC8-0 and YC10-0.

Correlation-length Spectrum.—While the energy gap is an important indication, the Dirac cone structure of the energy-momentum resolved spectrum will be a much stronger evidence of a DSL. So far, the study of a large number of excited states has been very challenging, but fortunately, recent seminal works [36,37] have uncovered a relationship between the energy spectrum and the spectrum of the transfer matrix in tensor-network formulation, which opens a window to the current problem.

The essence of this technique simply relies on a familiar fact: the information of excitations is encoded in the ground state, which can be decoded by measuring correlation functions of various operators. In infinite-DMRG simulations, the information of correlation functions of all operators can be straight-forwardly obtained through the eigenvalues of the transfer matrix [55]. Each eigenvalue takes the form $\lambda = e^{ik-1/\xi}$, where ξ is the corresponding correlation length and k is the momentum along the infinite-DMRG direction. The momentum around the cylinder can also be calculated from a revised transfer matrix [36]. The correlation lengths ξ set an upper bound for excitation gaps Δ (up to a nonuniversal factor), and for a Lorentz invariant system, it holds that $\Delta \propto 1/\xi$. One can make this statement precise by an exact mapping from the infinite-DMRG transfer matrix to the partition function in the Euclidean path integral [37]. In other words, if Lorentz (space-time rotation) symmetry is emergent in the system, the correlation-length spectrum precisely corresponds to the excitation spectrum of the Hamiltonian.

Figure 3 shows the $S^z = 1$ correlation-length spectrum of the J_1-J_2 TAFM at $J_2/J_1 = 0.12$. The left column shows the spectrum as a function of flux θ. Since θ effectively changes the quantization of the momenta, we can then obtain the full dispersion relation as a function of k_1 and k_2 in the two right columns. For the cylinders YC8/10-0 in Figs. 3(a) and 3(b), the Dirac cones at the M_2 point $(k_1, k_2) = (0, \pi)$ can clearly be identified (blue hexagon), corresponding to fermion bilinear excitations of type (**B3**) discussed above. In addition, there are low lying monopole excitations close to the $K_\pm$ points $(k_1, k_2) = (-2\pi/3, 2\pi/3)$ and $(2\pi/3, -2\pi/3)$ (red left triangle and magenta right triangle, respectively) of type (**M1**). For the cylinders YC8/10-1 in Figs. 3(c) and 3(d), we again find low lying excitations at the M point $(2k_1, k_2) = (0, \pi)$ (blue hexagon) and K points hexagon, $(-2\pi/3, -2\pi/3)$ (red left triangle and magenta right triangle). These observations of low lying excitations of fermion bilinear and monopole operators are clear evidence for a $U(1)$ DSL. We note that the lattice rotation symmetry C_6 is broken on the cylinder geometry, so its corresponding degeneracy is naturally split. In the Supplemental Material, a total of 16 different cylinder geometries are analyzed, which consistently show the predicted $U(1)$ DSL excitations [39].

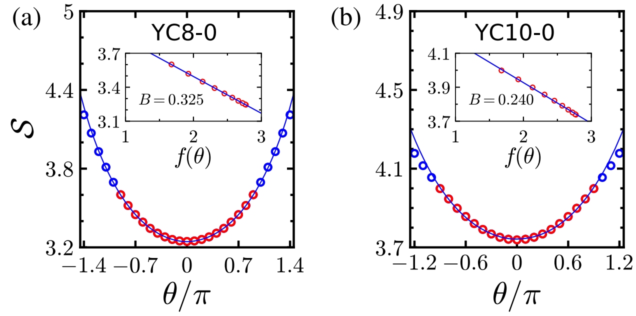

FIG. 4. Scaling behavior of the entanglement entropy. Entanglement entropy $\mathcal{S}$ (blue circles) as a function of flux θ for (a) YC8-0 ($m = 12288$) and (b) YC10-0 ($m = 8192$) cylinder geometries. Inset: Fit around minima to Eq. (2), where $f(\theta) = \sum_{n=1}^{N_f} \ln|2\sin[s(\theta - \theta_n^c)/2]|$. We fit the formula with data labeled by red circles.

Entanglement entropy.—Gapless spin liquids have nontrivial long-ranged quantum entanglement, in contrast to Landau ordered phases. Therefore, we also consider the bipartite entanglement entropy, $\mathcal{S} = -\mathrm{Tr}_{\mathrm{sys}}(\rho_{\mathrm{sys}} \ln \rho_{\mathrm{sys}})$, where the reduced density matrix $\rho_{\mathrm{sys}} = \mathrm{Tr}_{\mathrm{env}}(|\Psi\rangle\langle\Psi|)$ for the half-cylinder "system" is constructed by the ground-state wave function $|\Psi\rangle$ and traced over the degrees of freedom in the other half-cylinder "environment." It was recently proposed that the entanglement entropy of $2+1$D CFT may have a universal response to an external Aharonov-Bohm flux [56]. In particular, for DSL [38], we expect

$$\mathcal{S} = S_0(L_y) - B \sum_{n=1}^{N_f} \ln \left| 2\sin\left(\frac{s}{2}(\theta - \theta_n^c)\right)\right|, \qquad (2)$$

where $S_0(L_y)$ represents the area law part of entropy and B is a prefactor which may or may not be universal. Other parameters are universal and can be determined by the underlying theory: N_f accounts for the number of flavors of different Dirac spinons, $s = 1/2$ is the fractional spin carried by Dirac spinons, and θ_n^c corresponds to the flux value at which the nth Dirac spinon becomes gapless. This scaling function [Eq. (2)] has been successfully applied to identify the emergent DSL of the kagome antiferromagnet [38].

Figure 4 shows the flux dependence of the entanglement entropy $\mathcal{S}$ at $J_2/J_1 = 0.12$, which has a strong dependence on flux θ. This is a hallmark of low energy gapless excitations. In contrast, a fully gapped state would be largely insensitive to θ. Moreover, as shown in Fig. 4, the dependence of $\mathcal{S}$ on θ can be fitted by the scaling function Eq. (2) with parameters $N_f = 4$, $s = 1/2$, and $\theta_n^c = 2\pi$ for YC2n-0 and $\theta_n^c = \pm\pi$ for YC2n-1. This agrees well with our theoretical expectation.

Summary and discussion.—By combining large-scale DMRG simulations and recent analytical predictions, we study the intermediate spin liquid phase on the J_1-J_2 triangular antiferromagnetic Heisenberg model. Using flux insertion on different cylinder geometries, we demonstrate that the energy gap of the spin liquid closes, and more importantly, we find the low energy excitations of fermion bilinears and monopoles of the Dirac spin liquid. The simultaneous appearance of fermion bilinears and monopoles is in favor of a Dirac spin liquid scenario, as opposed to the scenario of proximity to an ordered phase. Moreover, the entanglement entropy response under flux insertion agrees with a universal scaling law of the Dirac spin liquid. These findings strongly suggest that the intermediate phase of the J_1-J_2 TAFM is a gapless Dirac spin liquid.

We thank Chong Wang for fruitful discussions. W. Z. is supported by start-up funding from Westlake University, and Project No. 11974288 under NSFC. S. J. H. and S. E. are supported by the German Research Foundation (DFG) via the Collaborative Research Center Grant No. SFB/TR185 (OSCAR). Research at Perimeter Institute (Y. C. H.) is supported by the Government of Canada through the Department of Innovation, Science and Economic Development Canada, and by the Province of Ontario through the Ministry of Research, Innovation, and Science. Especially, we gratefully acknowledge the Gauss Centre for Supercomputing e.V. (www.gauss-centre.eu) for funding this project by providing computing time through the John von Neumann Institute for Computing (NIC) on the GCS Supercomputer JUWELS at Jülich Supercomputing Centre (JSC).

[*]shijiehu@physik.uni-kl.de
[†]zhuwei@westlake.edu.cn
[‡]yinchenhe@perimeterinstitute.ca

[1] L. Savary and L. Balents, Quantum spin liquids: A review, Rep. Prog. Phys. **80**, 016502 (2016).

[2] Y. Zhou, K. Kanoda, and T.-K. Ng, Quantum spin liquid states, Rev. Mod. Phys. **89**, 025003 (2017).

[3] P. A. Lee, N. Nagaosa, and X.-G. Wen, Doping a Mott insulator: Physics of high-temperature superconductivity, Rev. Mod. Phys. **78**, 17 (2006).

[4] C. Broholm, R. J. Cava, S. A. Kivelson, D. G. Nocera, M. R. Norman, and T. Senthil, Quantum spin liquids, arXiv:1905.07040.

[5] P. W. Anderson, Resonating valence bonds: A new kind of insulator? Mater. Res. Bull. **8**, 153 (1973).

[6] S. Sachdev, Kagome- and triangular-lattice Heisenberg antiferromagnets: Ordering from quantum fluctuations and quantum-disordered ground states with unconfined bosonic spinons, Phys. Rev. B **45**, 12377 (1992).

[7] B. Bernu, C. Lhuillier, and L. Pierre, Signature of Néel Order in Exact Spectra of Quantum Antiferromagnets on Finite Lattices, Phys. Rev. Lett. **69**, 2590 (1992).

[8] L. Capriotti, A. E. Trumper, and S. Sorella, Long-Range Néel Order in the Triangular Heisenberg Model, Phys. Rev. Lett. **82**, 3899 (1999).

[9] W. Zheng, J. O. Fjærestad, R. R. P. Singh, R. H. McKenzie, and R. Coldea, Excitation spectra of the spin-$\frac{1}{2}$ triangular-lattice Heisenberg antiferromagnet, Phys. Rev. B **74**, 224420 (2006).

[10] S. R. White and A. L. Chernyshev, Neél Order in Square and Triangular Lattice Heisenberg Models, Phys. Rev. Lett. **99**, 127004 (2007).

[11] L. O. Manuel and H. A. Ceccatto, Magnetic and quantum disordered phases in triangular-lattice Heisenberg antiferromagnets, Phys. Rev. B **60**, 9489 (1999).

[12] R. V. Mishmash, J. R. Garrison, S. Bieri, and C. Xu, Theory of a Competitive Spin Liquid State for Weak Mott Insulators on the Triangular Lattice, Phys. Rev. Lett. **111**, 157203 (2013).

[13] R. Kaneko, S. Morita, and M. Imada, Gapless spin-liquid phase in an extended spin-1/2 triangular Heisenberg model, J. Phys. Soc. Jpn. **83**, 093707 (2014).

[14] Y. Iqbal, W.-J. Hu, R. Thomale, D. Poilblanc, and F. Becca, Spin liquid nature in the Heisenberg J_1-J_2 triangular antiferromagnet, Phys. Rev. B **93**, 144411 (2016).

[15] P. H. Y. Li, R. F. Bishop, and C. E. Campbell, Quasiclassical magnetic order and its loss in a spin-1/2 Heisenberg antiferromagnet on a triangular lattice with competing bonds, Phys. Rev. B **91**, 014426 (2015).

[16] W.-J. Hu, S.-S. Gong, W. Zhu, and D. N. Sheng, Competing spin-liquid states in the spin-1/2 Heisenberg model on the triangular lattice, Phys. Rev. B **92**, 140403(R) (2015).

[17] Z. Zhu and S. R. White, Spin liquid phase of the $S = 1/2$ J_1-J_2 Heisenberg model on the triangular lattice, Phys. Rev. B **92**, 041105(R) (2015).

[18] S. N. Saadatmand and I. P. McCulloch, Symmetry fractionalization in the topological phase of the spin-1/2 J_1-J_2 triangular Heisenberg model, Phys. Rev. B **94**, 121111(R) (2016).

[19] A. Szasz, J. Motruk, M. P. Zaletel, and J. E. Moore, Observation of a chiral spin liquid phase of the Hubbard model on the triangular lattice: A density matrix renormalization group study, arXiv:1808.00463.

[20] A. Wietek and A. M. Läuchli, Chiral spin liquid and quantum criticality in extended $S = \frac{1}{2}$ Heisenberg models on the triangular lattice, Phys. Rev. B **95**, 035141 (2017).

[21] S.-S. Gong, W. Zhu, J.-X. Zhu, D. N. Sheng, and K. Yang, Global phase diagram and quantum spin liquids in a spin-$\frac{1}{2}$ triangular antiferromagnet, Phys. Rev. B **96**, 075116 (2017).

[22] D.-V. Bauer and J. O. Fjærestad, Schwinger-boson mean-field study of the J_1-J_2 Heisenberg quantum antiferromagnet on the triangular lattice, Phys. Rev. B **96**, 165141 (2017).

[23] A. Yuste, D. Castells-Graells, and A. Sanpera, Signatures of quantum spin liquids in small lattices, Phys. Rev. B **100**, 155119 (2019).

[24] F. Ferrari and F. Becca, Dynamical Structure Factor of the J_1-J_2 Heisenberg Model on the Triangular Lattice: Magnons, Spinons, and Gauge Fields, Phys. Rev. X **9**, 031026 (2019).

[25] T. Jolicoeur, E. Dagotto, E. Gagliano, and S. Bacci, Ground-state properties of the S = 1/2 Heisenberg antiferromagnet on a triangular lattice, Phys. Rev. B **42**, 4800 (1990).

[26] A. V. Chubukov and T. Jolicoeur, Order-from-disorder phenomena in Heisenberg antiferromagnets on a triangular lattice, Phys. Rev. B **46**, 11137 (1992).

[27] Z. Zhu, P. A. Maksimov, S. R. White, and A. L. Chernyshev, Topography of Spin Liquids on a Triangular Lattice, Phys. Rev. Lett. **120**, 207203 (2018).

[28] P. A. Maksimov, Z. Zhu, S. R. White, and A. L. Chernyshev, Anisotropic-Exchange Magnets on a Triangular Lattice: Spin Waves, Accidental Degeneracies, and Dual Spin Liquids, Phys. Rev. X **9**, 021017 (2019).

[29] M. Baenitz, P. Schlender, J. Sichelschmidt, Y. A. Onykiienko, Z. Zangeneh, K. M. Ranjith, R. Sarkar, L. Hozoi, H. C. Walker, J.-C. Orain, H. Yasuoka, J. van den Brink, H. H. Klauss, D. S. Inosov, and T. Doert, $NaYbS_2$: A planar spin-$\frac{1}{2}$ triangular-lattice magnet and putative spin liquid, Phys. Rev. B **98**, 220409(R) (2018).

[30] W. Liu, Z. Zhang, J. Ji, Y. Liu, J. Li, X. Wang, H. Lei, G. Chen, and Q. Zhang, Rare-Earth chalcogenides: A large family of triangular lattice spin liquid candidates, Chin. Phys. Lett. **35**, 117501 (2018).

[31] L. Ding, P. Manuel, S. Bachus, F. Gruβler, P. Gegenwart, J. Singleton, R. D. Johnson, H. C. Walker, D. T. Adroja, A. D. Hillier, and A. A. Tsirlin, Gapless Spin-Liquid State in the Structurally Disorder-Free Triangular Antiferromagnet $NaYbO_2$, arXiv:1901.07810 [Phys. Rev. Lett. (to be published)].

[32] K. M. Ranjith, D. Dmytriieva, S. Khim, J. Sichelschmidt, S. Luther, D. Ehlers, H. Yasuoka, J. Wosnitza, A. A. Tsirlin, H. Kühne *et al.*, Field-induced instability of the quantum spin liquid ground state in the $J_{\mathrm{eff}} = \frac{1}{2}$ triangular-lattice compound $NaYbO_2$, Phys. Rev. B **99**, 180401(R) (2019).

[33] M. Bordelon, E. Kenney, T. Hogan, L. Posthuma, M. Kavand, Y. Lyu, M. Sherwin, C. Brown, M. J. Graf, L. Balents, and S. D. Wilson, Field-tunable quantum disordered ground state in the triangular lattice antiferromagnet $NaYbO_2$, Nat. Phys. **15**, 1058 (2019).

[34] X.-Y. Song, C. Wang, A. Vishwanath, and Y.-C. He, Unifying description of competing orders in two dimensional quantum magnets, Nat. Commun. **10**, 4254 (2019).

[35] X.-Y. Song, Y.-C. He, A. Vishwanath, and C. Wang, From spinon band topology to the symmetry quantum numbers of monopoles in Dirac spin liquids, arXiv:1811.11182.

[36] Y.-C. He, M. P. Zaletel, M. Oshikawa, and F. Pollmann, Signatures of Dirac Cones in a DMRG Study of the Kagome Heisenberg Model, Phys. Rev. X **7**, 031020 (2017).

[37] V. Zauner, D. Draxler, L. Vanderstraeten, M. Degroote, J. Haegeman, M. M. Rams, V. Stojevic, N. Schuch, and F. Verstraete, Transfer matrices and excitations with matrix product states, New J. Phys. **17**, 053002 (2015).

[38] W. Zhu, X. Chen, Y.-C. He, and W. Witczak-Krempa, Entanglement signatures of emergent Dirac fermions: Kagome spin liquid and quantum criticality, Sci. Adv. **4**, eaat5535 (2018).

[39] See Supplemental Material at http://link.aps.org/supplemental/10.1103/PhysRevLett.123.207203 for discussion of Dirac spin liquid, numerical procedure, and additional supporting numerical data on different geometries, which includes Refs. [16–18,21,36–38, 40–42].

[40] Y.-C. He, D. N. Sheng, and Y. Chen, Obtaining topological degenerate ground states by the density matrix renormalization group, Phys. Rev. B **89**, 075110 (2014).

[41] S.-S. Gong, W. Zheng, M. Lee, Y.-M. Lu, and D. N. Sheng, Gapless chiral spin liquid phase in spin-1/2 triangular Heisenberg model, arXiv:1905.11560.

[42] F. Pollmann, S. Mukerjee, A. M. Turner, and J. E. Moore, Theory of Finite-Entanglement Scaling at One-Dimensional Quantum Critical Points, Phys. Rev. Lett. **102**, 255701 (2009).

[43] Y. Zhou and X.-G. Wen, Quantum orders and spin liquids in Cs_2CuCl_4, arXiv:cond-mat/0210662.

[44] M. Hermele, T. Senthil, M. P. A. Fisher, P. A. Lee, N. Nagaosa, and X.-G. Wen, Stability of $U(1)$ spin liquids in two dimensions, Phys. Rev. B **70**, 214437 (2004).

[45] M. Hermele, T. Senthil, and M. P. A. Fisher, Algebraic spin liquid as the mother of many competing orders, Phys. Rev. B **72**, 104404 (2005).

[46] M. Hermele, Y. Ran, P. A. Lee, and X.-G. Wen, Properties of an algebraic spin liquid on the kagome lattice, Phys. Rev. B **77**, 224413 (2008).

[47] T. Giamarchi, *Quantum Physics in One Dimension* (Oxford University Press, Oxford, 2003).

[48] I. Affleck, Fields, Strings and Critical Phenomena, in *Fields, Strings and Critical Phenomena*, edited by E. Brézin and J. Zinn-Justin (Les Houches 1988, Proceedings, North-Holland, 1988), Vol. 49, pp. 563–640.

[49] S. Eggert and I. Affleck, Magnetic impurities in half-integer-spin Heisenberg antiferromagnetic chains, Phys. Rev. B **46**, 10866 (1992).

[50] J. Alicea, Monopole quantum numbers in the staggered flux spin liquid, Phys. Rev. B **78**, 035126 (2008).

[51] S. R. White, Density Matrix Formulation for Quantum Renormalization Groups, Phys. Rev. Lett. **69**, 2863 (1992).

[52] S. R. White, Density-matrix algorithms for quantum renormalization groups, Phys. Rev. B **48**, 10345 (1993).

[53] I. P. McCulloch, Infinite size density matrix renormalization group, revisited, arXiv:0804.2509.

[54] The gap obtained at $\theta = 0$ is consistent with previous results. For example, for the YC8-1 (YC8-0) cylinder a spin triplet gap of $\Delta_{S^z=1} \approx 0.3J_1$ $(0.4J_1)$ is found, close to previous results for $J_2/J_1 = 0.125$ [21] and $J_2/J_1 = 0.1$ [17].

[55] U. Schollwöck, The density-matrix renormalization group in the age of matrix product states, Ann. Phys. (Amsterdam) **326**, 96 (2011).

[56] X. Chen, W. Witczak-Krempa, T. Faulkner, and E. Fradkin, Two-cylinder entanglement entropy under a twist, J. Stat. Mech. (2017) 043104.